Timing of paraglacial rock-slope failures and denudation signatures in the Cantabrian Mountains (North Iberian Peninsula)

Laura Rodríguez-Rodríguez[a, b*], Saúl González-Lemos[a], Daniel Ballesteros[a, c], Pablo Valenzuela[a], María José Domínguez-Cuesta[a], Sergio Llana-Fúnez[a], Montserrat Jiménez-Sánchez[a]

[a]*Departamento de Geología, Universidad de Oviedo, Arias de Velasco s/n, 33005 Oviedo, Spain,*

[b] *Laboratoire de Géographie Physique (UMR 8591, CNRS), 1 Place Aristide Briand, 92195 Meudon CEDEX, France,*

[c] *Université de Rouen (UMR IDEES 6266), Mount Saint-Aignan, 76130 Rouen, France.*

*

Abstract

Glacial erosion of hillslopes and stress changes induced by the transition from glacial to nonglacial conditions exert a strong influence on slope instability and are considered among the scope of paraglacial geomorphology. Failure mechanisms and coupling between paraglacial rock-slope failures (RSFs) and fluvial erosion are difficult to define. Here we show a preliminary spatio-temporal framework of paraglacial RSFs in a small catchment of the central Cantabrian Mountains, the San Isidro valley, with a dense concentration of RSFs. Preliminary radiocarbon dates obtained from two floodplain sequences deposited upstream from RSFs indicate that their sedimentation started as consequence of valley impoundment by RSFs after glacier retreat (after approximately 16.1 ka), consistent with the deglaciation pattern of nearby valleys. RSFs continued during the Holocene. Glacier erosion, debuttressing, and stress-release conditions played an important role on slope destabilization as preparatory factors in all cases, and probably triggered the oldest events. However, the long prefailure endurance (approximately 12 ka) between RSFs points to other factors such as rainfall and fluvial down-cutting of hillslopes as triggers for Holocene events. Postglacial fluvial incision rates of 2.2-2.5 mm a^{-1} were estimated along gullies carved into bedrock areas non-affected by RSFs. These values are one order of magnitude higher than previous rates based on other geomorphological proxies (~ 0.2 mm a^{-1}), suggesting accelerated fluvial incision following the last deglaciation. Local RSFs contributed to increase in fluvial incision rates by a factor of three. This study provides a quantitative perspective of postglacial land degradation relevant for understanding postorogenic landscape evolution.

Key words

Cantabrian Mountains, denudation rate, landslide, paraglacial processes, rock-slope failure.

1. Introduction

Paraglacial geomorphology is the study of Earth-surface processes, landforms, sediments, and landscapes directly conditioned by former glaciation and deglaciation (Ballantyne, 2002). According to Slaymaker (2011), paraglacial environments retain a glacial signature in their configuration and are out of adjustment with contemporary process. Rock-slope failures (RSFs) are slope destabilizations that directly modify bedrock topography and typically occur in formerly-glaciated landscapes, where they are often termed 'paraglacial' (Ballantyne & Stone, 2013). In deglaciated landscapes, RSFs might be included in the scope of paraglacial geomorphology because they are part of, or influenced by, the transition from glacial to non-glacial conditions (McColl, 2012). Glaciers induce deep changes in preglacial landscape topography. In particular, glacier tongues are responsible for enhanced erosion of hillslopes and valley floors, resulting in cross-section widening and valley floor flattening (Whipple, Kirby, & Brocklehurst, 1999). The clustered distribution of landslides above trimlines in the British Columbia suggests that both changes in slope form and loss of lateral buttressing (i.e. glacial debuttresing) of slopes due to glacier retreat increase the probability of slope failure (Dadson & Church, 2005). Cossart, Braucher, Fort, Bourlès, and Carcaillet (2008) found that RSFs in the French Alps are clustered within areas where ice load stresses were higher, confirming that glacial debuttresing and stress release played a key role as failure triggers. However, chronological studies on the temporal distribution of RSFs have shown that most slopes typically failed a few hundred years to several millennia after deglaciation (McColl, 2012), suggesting the possible implication of progressive failure mechanisms or other triggering factors such as seismic activity or climate change (Ivy-Ochs et al., 2008; Lebourg, Zerathe, Fabre, Giuliano, & Vidal, 2014; Nagelisen, Moore, Vockenhuber, & Ivy-Ochs, 2015; Pánek et al., 2016). Based on ^{10}Be cosmogenic isotope dating of 89 boulders from RSF in Ireland and Scotland, Ballantyne, Sandeman, Stone, and Wilson (2014) concluded that RSFs have spanned the whole period since ice-sheet retreat, being ca. 4.6 times more frequent prior to ca. 11.7 ka and extending with a low frequency throughout the Holocene. Another study in Northern Ireland relying on ^{36}Cl cosmogenic isotope and radiocarbon dating indicates that most RSFs occurred during or immediately following deglaciation (18-17 ka), while some ages suggest some smaller scale events during the Lateglacial and/or early Holocene (14 to 9 ka; Southall et al., 2017). Similarly, a recent study in Iceland suggests that 94% of RSFs investigated occurred prior to 10 ka, whereas later events occurred before 8 ka, being difficult to identify the final trigger for each individual event (Mercier et al., 2017).

Paraglacial slope instabilities constitute a key mechanism for fast degradation of recently glacial landscapes, as they contribute to the disaggregation of large portions of the valley sides that can then be more easily eroded by fluvial processes if landslide deposits are coupled with streams (Cossart, Mercier, Decaulne, & Feuillet, 2013). The stochastic model developed by Dadson and Church (2005) and calibrated with field data from British Columbia (Canada) shows that fluvial sediment transport is high for a long period after glacier retreat (approximately 10 ka) and the distribution of channels is strongly controlled by hillslope processes. Recent studies have focused their efforts on quantifying paraglacial land degradation through a combination of slope and fluvial processes. Vehling et al. (2017) used multi-temporal terrestrial and airborne LiDAR observations to determine sediment transport by gravitational mass movements in the Austrian Alps. In the same mountain region, Kellerer-Pirklbauer, Proske, and Strasser (2010) combined field data, laboratory analysis, aerial photographs, and GIS-based terrain analyses to calculate linear erosion rates in the range 0.5 to 2.6 mm a^{-1} from gullies carved in the lower part of a deep-seated landslide. Although paraglacial landslides dismantle mountain slopes after deglaciation and provide large amounts of debris that can reach the valley bottom, they often act as persistent dams and only particular settings (e.g. very active orogens with high uplift rate) may ensure sediment transfers (Cossart et al., 2013). In this work we focus on a small high mountain valley of the Cantabrian Mountains in North Iberian Peninsula that displays a dense clustering of RSFs. Most of them have reached the valley bottom, promoting temporal damming of the valley and development of floodplains. Unlike the Pyrenees, where detailed inventories of RSFs deposits are available (Jarman, Calvet, Corominas, Delmas, & Gunnell, 2016), the exact distribution of paraglacial RSFs remains poorly defined and little information is known on the timing distribution and factors involved in their occurrence. Because of the clear linkage between paraglacial slope instabilities and fluvial processes and the good chronological constraint for the transition from glacial to periglacial conditions in the region, this mountain valley provides an opportunity to investigate the interplay between RSF events and fluvial incision rates. Thus, the aim of this contribution is: (i) to constrain the timing and failure causes of RSFs in formerly glaciated areas of the Cantabria Mountains in North Iberian Peninsula; and (ii) to quantify post-glacial denudation rates due to a combination of slope and fluvial processes.

2. Regional setting

The San Isidro valley is located in the northern slope of the central Cantabrian Mountains, a mountain range with a top elevation of 2648 m asl disposed parallel to the North coastline of the Iberian Peninsula (approximately 43ºN latitude; Figure 1a). Particularly, the San Isidro valley is a mountain valley that belongs to the headwater area of the Aller river basin in Asturias (North Spain). The study area corresponds to a 5.4 km-long creek that flows between the Fuentes de Invierno ski area (1666 m asl) and Riofrío (1200 m asl), showing an average slope of 4.9º. The wetted width of Braña Creek varies from 5 to < 2 m during low water level conditions (July to September) and up to 7 m during the snowmelt season (April to June). According to the Köppen-Geiger classification for the Iberian Peninsula, the Cantabrian Mountains lowlands show a temperate climate without dry season and temperate summer (*Cfb*), while the highlands mostly present a temperate climate with dry/temperate summer season (C*sb*). Only the highest areas of the mountain range display a cold climate regime characterized by either temperate/dry (*Dsb*) and dry/fresh (*Dsc*) summers (García-Couto, 2011). Precipitation and temperature patterns in the study valley are characterized by average annual values of 1292 mm (1972-1995 period) and 5.7 ºC (1970-1995 period), respectively, considering data from an AEMET weather station at the vicinity of the San Isidro Pass (UTM coordinates: 306447X–4770738Y; 1540 m asl; http://sig.mapama.es/siga/visor.html; last accessed on August 2017). The thickness of the snow mantle varied from 1 to 4 m over the period 2009-2016 according to datasets from the Fuentes de Invierno ski area (https://www.infonieve.es/estacion-esqui/fuentes-de-invierno/historico-nieve/; last accessed on December 2017).

Geologically, the San Isidro valley is located in the Cantabrian Zone of the Iberian Massif, particularly in the Bodón-Ponga Unit (Alonso, Marcos, & Suárez, 2009). Bedrock is composed by alternations of Paleozoic detrital and carbonate formations affected by thrusts and folds ascribed to the Variscan Orogeny (380 to 280 Ma; Julivert, 1971; Pérez-Estaún et al., 1988). The Alpine orogeny uplifted the Cantabrian Mountains between the Upper Cretaceous and the Miocene (Alonso, Pulgar, García-Ramos, & Barba, 1996; Marquínez, 1992; Pulgar et al., 1996), while post-orogenic uplift continued during the Pliocene and thereafter (Álvarez-Marrón, Hetzel, Niedermann, Menéndez, & Marquínez, 2008; Jiménez-Sánchez, Bischoff, Stoll, & Aranburu, 2006; Viveen, Schoorl, Veldkamp, & van Balen, 2014). The San Isidro valley is mostly carved in soft rock materials of Beleño Formation (Bashkirian sandstone, shale and limestone alternations; Figure 1b) and shows an E-W trend following the San Isidro Antiform (Álvarez-Marrón, Heredia, & Pérez-Estaún, 1989). The north and south watersheds correspond to hard rocks such as Barrios Formation (Cambro-Ordovician quartzite sandstone) and Escalada Formation (Moscovian limestone) and constitute the fold limbs of the San Isidro Antiform (Figure 1c). Both slopes of the San Isidro valley are E-W oriented and parallel to the strike of bedrock bedding, which is subvertically disposed.

Quaternary glaciations extensively contributed to shape the San Isidro valley, sculpting glacial cirques along the north and south watersheds and the San Isidro valley, which typical has a U-shaped section that is only preserved at the Riofrío bedrock threshold (1200 m asl). During the local glacial maximum stage, glaciers flowed down to the Riofrío bedrock threshold, where a slope break approximately 170 m high would have conditioned the formation of a serac (Rodríguez-Pérez, 1995). Numerical reconstruction of former glaciers in this valley estimates that ice thickness reached maximum values of 150-200 m along the center flow line of the valley, and the equilibrium line altitude was at a mean elevation of 1642 ± 26 m (area-altitude balande ratio method considering multiple balance ratio values ranging from 1 to 3) during the local glacial maximum stage (Rodríguez-Rodríguez, 2015). The transition from glacial to non-glacial conditions led to periglacial activity evidenced by relict rock glaciers preserved in the north facing cirques of the Fuentes de Invierno Range (Gómez-Villar, González-Gutiérrez, Redondo-Vega, & Santos-González, 2011). The timing of the last deglaciation in this region was constrained on the basis of ^{10}Be cosmic-ray exposure dating applied to moraine and rock glacier boulders in the nearby Porma basin. Results suggest that glaciers were retreating by 17.7 ± 0.4 ka, whereas the frontal ridge of some rock glaciers stabilized by 15.7 ± 0.3 ka (Rodríguez-Rodríguez et al., 2016).

3. Methods

Methods applied in this work combine an estimate of landscape changes induced by RSFs and radiocarbon dating of RSF-dammed floodplains in order to constrain the paraglacial evolution of the San Isidro valley. Landscape changes were quantified based on geomorphological mapping and spatial analysis of digital elevation models (DEMs). The identification of landforms was based on field work observations attending to topography and sedimentology criteria. Geomorphological map production was supported by interpretation of aerial photographs and airborne LiDAR datasets from the Spanish Instituto Geográfico Nacional (available online at https://www.cnig.es/; last access on July 2017). Once uncompressed, LiDAR datasets were filtered by ground and used to derive (a) 2-m cell-size resolution DEM, (b) 2-m cell-size resolution digital hillshade model (DHM), and (c) 5-m-spaced contour line topographic map. Geomorphological evidence in the San Isidro valley was mapped and digitized in a geographical information system to produce a geomorphological map at a 1:10,000 scale. The use of high-resolution, airborne LiDAR-based, ground-filtered digital terrain models greatly helped to map vegetation-covered landforms such as rock glaciers and RSFs in the southern slope of the San Isidro valley.

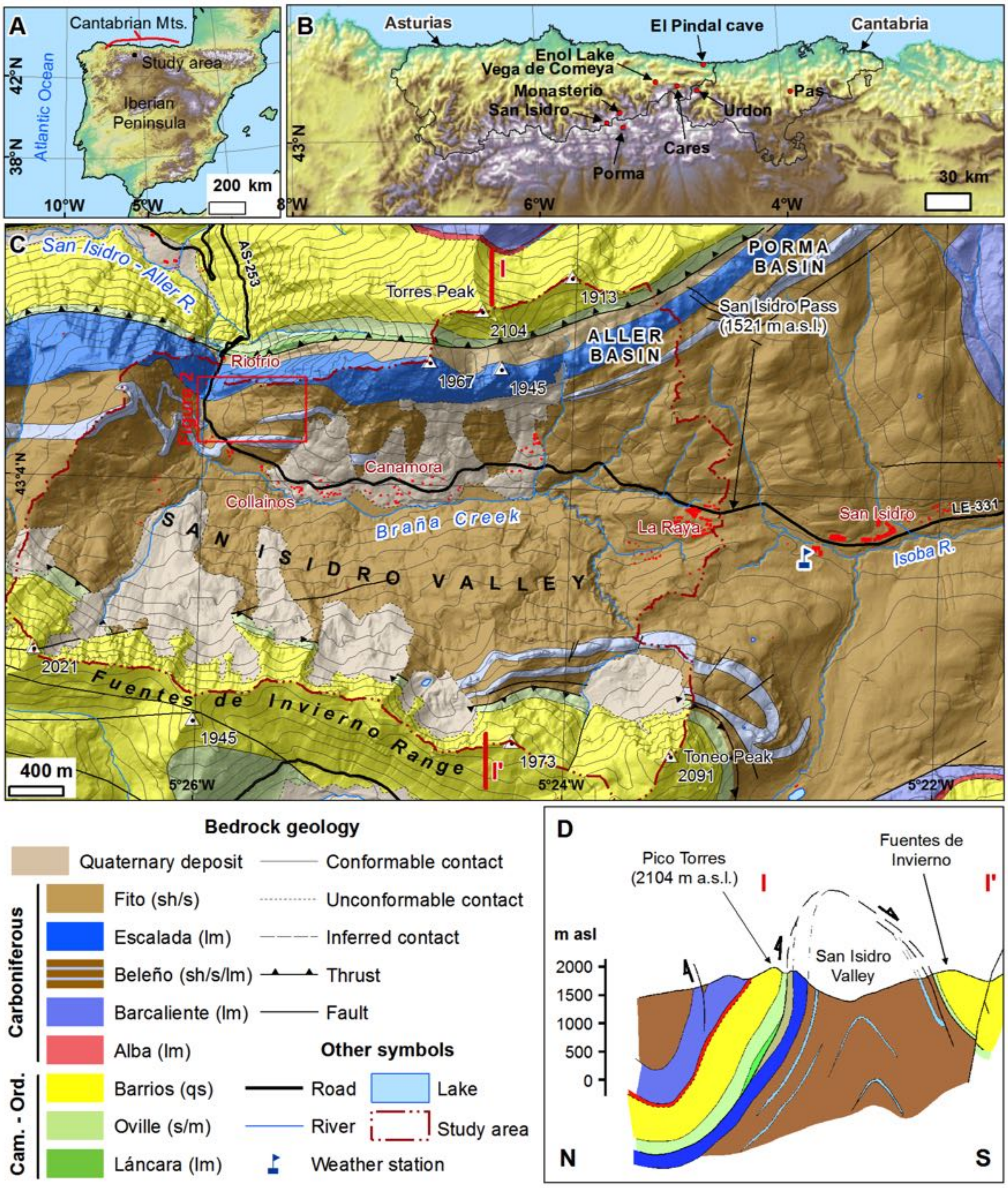

Figure 1.- (a) Geographic location of the Cantabrian Mountains and the study area in the context of the Iberian Peninsula. (b) Location of the study area in the Cantabrian Mountains, as well as other sites

mentioned in the text. (c) Bedrock geology compiled in Merino-Tomé et al. (2011): sh, shale; s, sandstone; qs- quartzite sandstone; lm, limestone. (d) Geologic cross section of the San Isidro valley.

The timing of paraglacial RSFs in the San Isidro valley was investigated by applying radiocarbon dating to alluvial sediments deposited in close relation to slope failure events. Two sediment cores (named Canamora-01 and Canamora-02) were drilled with a manual sampler manufactured by Eijelkamp® in two different floodplains deposited upstream the main bodies of several RSFs due to the valley damming effect of RSFs. The sedimentary sequence of both cores was described and sampled for radiocarbon dating, providing minimum reference ages for paraglacial RSFs, valley impoundment and floodplain sedimentation. Five radiocarbon samples were analyzed at Poznan Radiocarbon Laboratory (Poland), and the results were calibrated with the Radiocarbon Calibration Program Calib Rev 7.0.2 and the IntCal13 curve (Reimer et al., 2013; Stuiver & Reimer, 1993).

In order to estimate the erosive signature in the San Isidro valley induced by paraglacial RSFs, a polygon shapefile enclosing both the main body and the head scarp of each RSF was created. Polygon vertices corresponding to the limit between affected and non-affected hillslope topography were extracted and combined with the LiDAR-based DEM using the ArcGIS tools 'Feature vertices to points' and 'Extract values to points' (Figure 2a). Resultant elevation points were used to interpolate the post-glacial surface topography of both valley sides before the occurrence of paraglacial RSFs through the 'Topo to raster' command (Figure 2b). The high-resolution airborne LiDAR-based DEM of modern topography was resampled to get the same resolution considered in the pre-RSF topographic restitution (10-m cell-size resolution). Restored and modern topographic surfaces were compared with the 'cut and fill' command in order to quantify net volume losses and gains attributed to RSFs (Figure 2c).

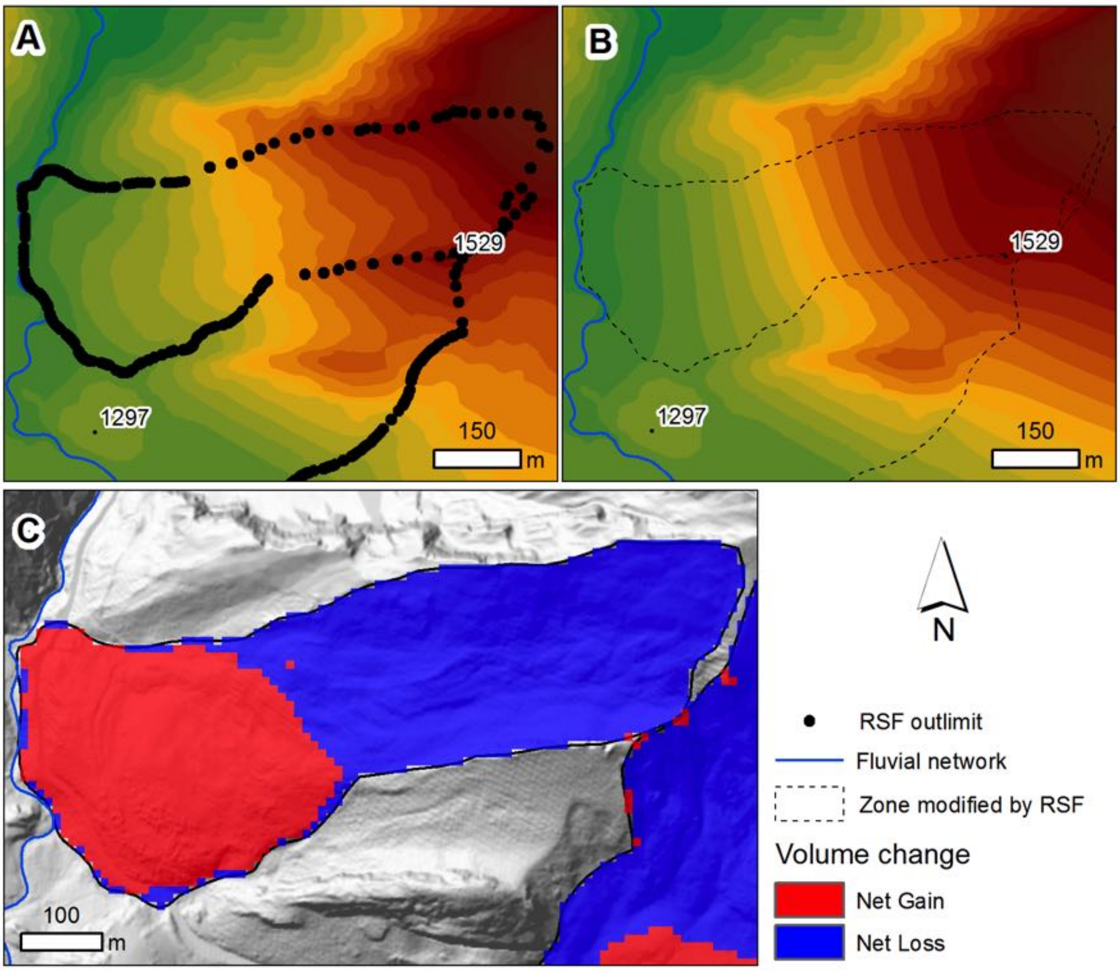

Figure 2.- Example of surface topography restitution of a hillslope affected by rock-slope failures (RSFs): (a) Current topography and out limit point elevations derived from the RSF polygon shape (20-m-spaced digital elevation model [DEM]). (b) Pre-RSF hillslope topography (10-m cell-size resolution) restituted with the topo to raster command (20-m-spaced DEM). (c) Volume changes occurred in destabilized hillslopes (10-m cell-size resolution) quantified by the cut and fill command.

4. Results

4.1. Geomorphology and landform assemblages

The study area (13.1 km^2) includes topographic elevations over 1200 m asl and shows landforms related to glacial, periglacial, slope, and alluvial/lacustrine processes (Figure 3). Glacial erosive landforms include ten glacial cirques, eight carved in the northern slope of Fuentes de Invierno Range and two carved in the southern side of Torres Peak (2104 m asl), and a well-defined U-shaped valley section at the Riofrío bedrock threshold, at the base level of the study area (Figure 4a). Glacial depositional landforms mostly correspond to lateral to frontal moraines preserved along the southern and western hillslopes of the San Isidro valley at altitudes between 1400 and 1800 m asl and show low and rounded ridge sections. Also, quartzite sandstone erratic boulders (Barrios Formation) have been found resting on top of the Escalada limestone, hanging approximately 80 m above the valley floor (Figure 4b). Erratic boulders are ascribed to the Pleistocene local glacial maximum, while moraines are mostly ascribed to recessional stages deposited when glaciers were retreating. Rock glaciers and peat bogs are frequently nested within moraines (Figure 4c). Rock glaciers only developed along the northern slope of Fuentes de Invierno Range, displaying their initiation line between 1700 and 1800 m altitude and their frontal ridge between 1520 and 1700 m asl. They are composed by angular quartzite sandstone boulders (mostly from the Barrios Formation) and are characterized by multiple concentric ridge-trough topography. On the basis of their plan view morphology, Gómez-Villar et al. (2011) classified them as tongue-shape, lobate, and complex rock glaciers. The use of high-resolution airborne LiDAR-based DEMs allowed the observation of clear cross-cutting relationships between rock glaciers and RSFs in the southern valley side not clearly identified in previous works (Gómez-Villar et al., 2011; Rodríguez-Pérez, 1995; Suárez-Rodríguez, 1987; Figure 3). The ridge-trough topography of rock glaciers is clearly interrupted by concave RSF scars 45 to 70 m high, and the lowest part of affected rock glaciers is incorporated and mixed into the RSF deposits. Slope instability landforms represent approximately 25% of the total study area and include RSFs (17%) that deeply modified original bedrock topography, but also talus scree (6%) and colluvial deposits (2%). Table 1 compiles the dimensions and typology of RSFs deposits identified in the geomorphological map. RSFs distributed along the north valley side mostly correspond to rock avalanches (IDs 1, 2, 4 and 6; see Figure 3 and

Table 1) and show concave head scarps extending up to the water divide and affecting both limestone (Fm. Escalada) and sandstone-shale rocks (Fm. Beleño). Only two complex landslides (IDs 3 and 5) were identified on this hillslope, affecting just the sandstone-shale rocks of the Beleño Formation and with their head scarp at lower elevations (1500-1640 m). In contrast, all RSFs identified in the southern hillslope corresponds to complex landslides (IDs 8 to 15) affecting the sandstone-shale rocks of the Beleño Formation, with the exception of a small rock avalanche located north of the Fuentes de Invierno ski area, which involves limestone boulders from a strata imbedded within the Beleño Formation (ID 7). Head scarps of RSFs distributed along the southern hillslope initiate at 1400-1650 m altitude, where they show clear cross-cutting relationships with moraines and rock glaciers (Figure 5). The bottom of the San Isidro valley shows three floodplains with surface extent in the range 3.8 to 4.4 ha. In all cases they are located upstream from RSFs at altitudes of approximately 1270, 1320 and 1355 m asl, so they are interpreted as deposited due to the impoundment of the valley by RSF events. The toe areas of RSFs are affected by fluvial erosion, showing scarps with height of up to 27 ± 5 m. Meandering gullies in the north face of Toneo Peak (2091 m asl) also evidence enhanced fluvial erosion, showing depth values of 37 ± 12 m.

The following relative age relationships are observed for RSF events in the San Isidro valley on the basis of their cross-cutting and superimposition relationships; topography preservation of RSF body and head scarp areas; and differences in vegetation density cover.

1. RSFs 11/9 prior to 10: they show poorly preserved scarps and are the most densely vegetated of the group. Their toe zones show rectilinear morphology due to intense postdepositional erosion, and they are superimposed by RSF 10.

2. RSF 3: it is superimposed by RSF 4. It could have occurred in response to fluvial down-cutting in the northern hillslope as a consequence of RSF 11.
3. RSFs 4/6 prior to 5: 4 and 6 could have occurred very close in time given geometric and topographic similarities between their toes and head scarps. Also, both present well-developed debris slope coverage on top. They were followed by RSF 5 whose scarp cuts the body of RSF 4 and superimposes the bodies of RSFs 4 and 6.
4. RSF 2 prior to 1: the highest portion of RSF 1 scarp cuts the scarp of RSF 2. It is difficult to place in time RSFs 1 and 7 compared to RSFs 4 and 6, and they could have occurred closely in time. RSF 7 developed from a vertical scarp and is spatially isolated from the rest of the group. The toe of RSF 2 promoted the southward migration of the Braña Creek, and probably triggered RSF 12 by fluvial down-cutting of the slope.
5. RSFs 13 prior to 12/14 and 15: the density of the vegetation coverage is very similar, but geometrically, RSF 12 superimposes RSF 13. Also, RSF 13 is cut by RSF 14, while RSF 15 cuts RSF14.
6. RSF 10 prior to 8: they are smaller than most RSFs and display the best preserved and less vegetated head scarps of the whole sequence. Comparatively, the scarp of RSF 8 is less vegetated than in RSF 10.

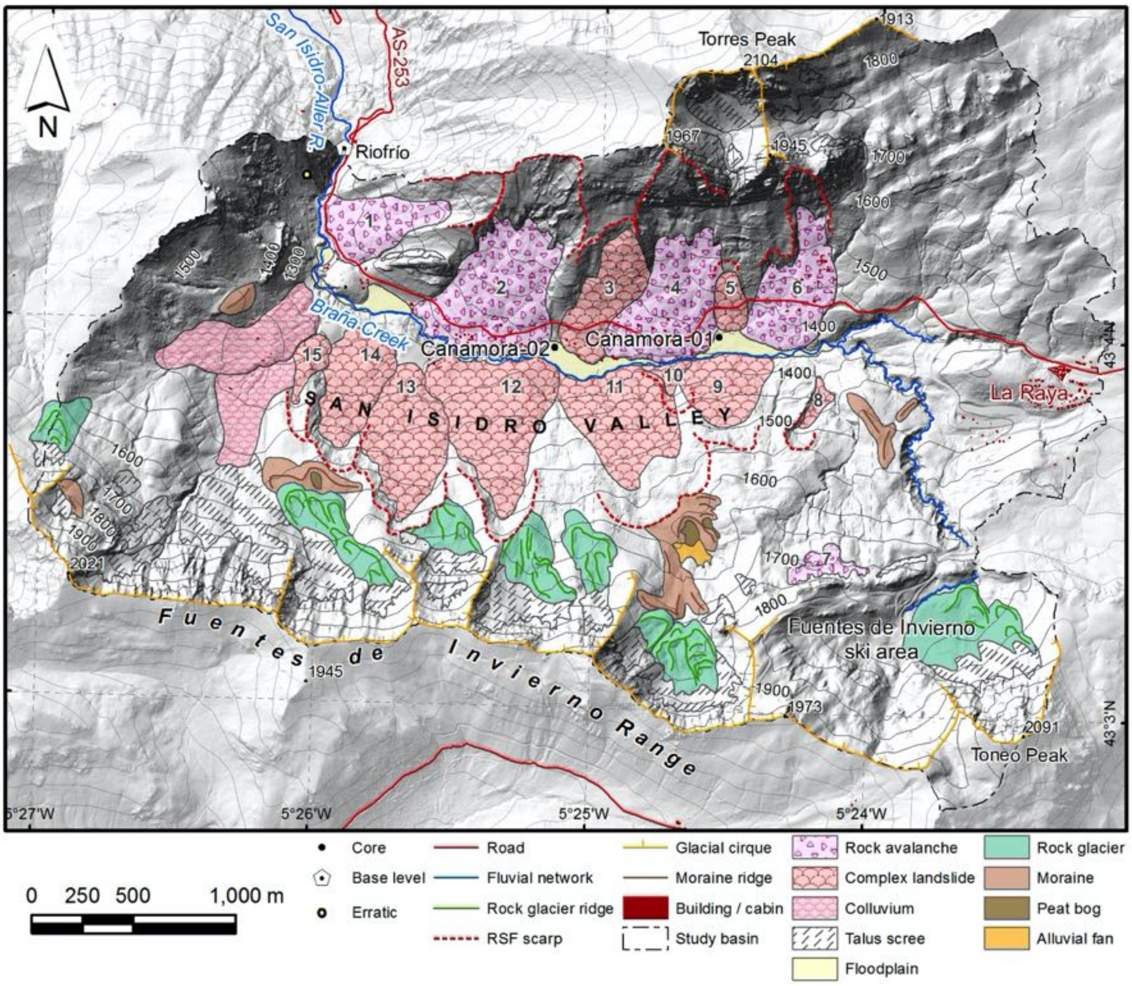

Figure 3.- Geomorphological map of the San Isidro valley showing the location of both sediment cores (Canamora-01 and Canamora-02) and rock-slope failures (ID numbering corresponds to Table 1).

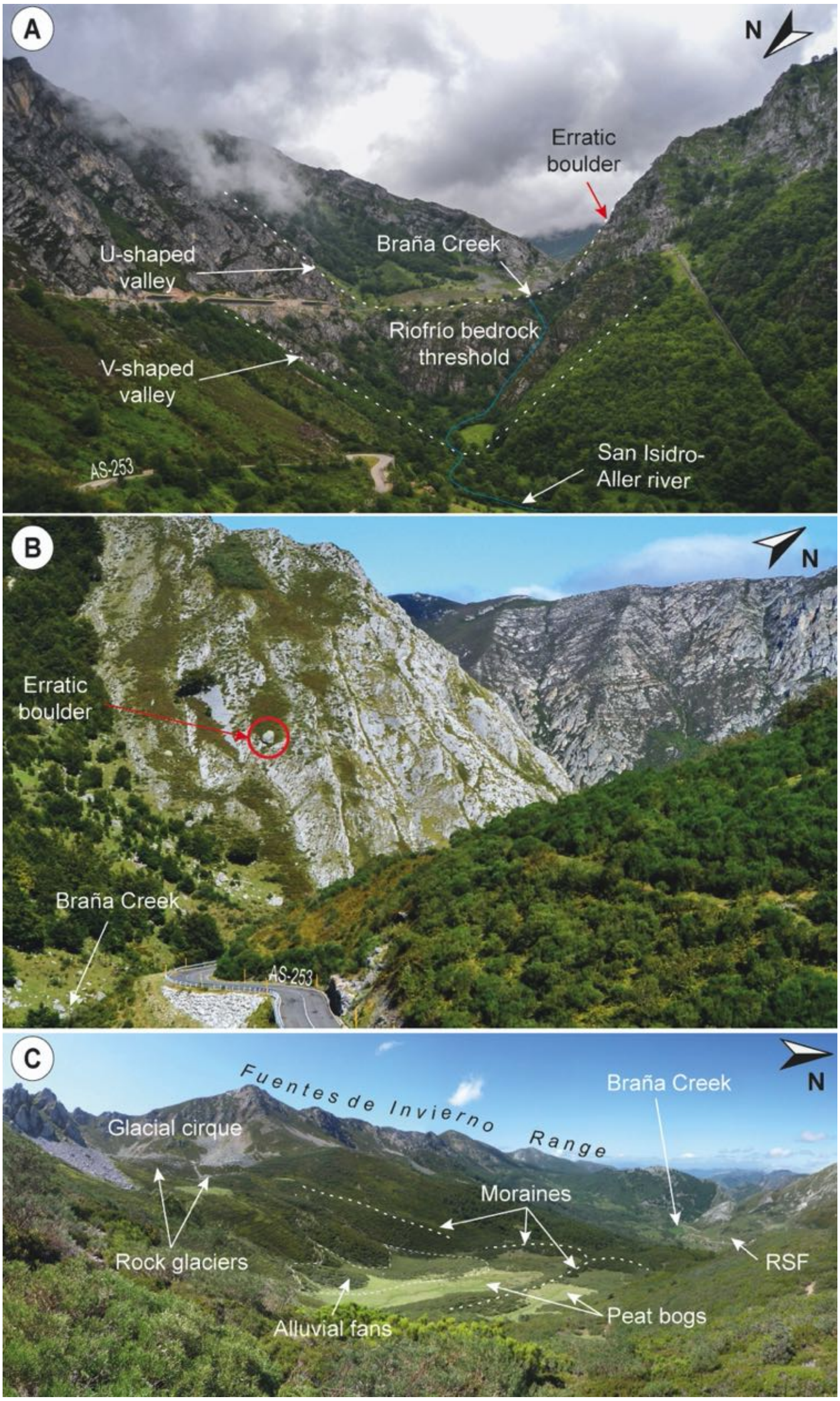

Figure 4.- (a) U-shaped valley section preserved at the base level of the study area (1200 m asl). (b) Erratic boulder of quartzite sandstone (circled in red) preserved on limestone bedrock and hanging approximately 80 m respect to the San Isidro valley floor. (c) Geomorphic evidence preserved in the northern slope of Fuentes de Invierno Range.

Table 1. Dimensions of RSFs in the study area (locations are shown in figure 3).

ID	RSF type	Length (m)	Width (m)	Area (m^2)	Volume (m^3)	Relative sequence
1	Rock avalanche	656	374	140,012	1,428,122	III?
2	Rock avalanche	740	695	315,571	3,218,824	IV
3	Complex landslide	687	290	143,894	1,467,719	II
4	Rock avalanche	619	538	248,101	2,530,630	III
5	Complex landslide	286	163	39,504	402,941	IV
6	Rock avalanche	708	392	185,280	1,889,856	III
7	Rock avalanche	147	403	35,938	366,568	III?
8	Complex landslide	223	134	16,174	164,975	VIII
9	Complex landslide	358	401	117,366	1,197,133	I
10	Complex landslide	152	249	17,262	176,072	VII
11	Complex landslide	597	555	231,510	2,361,402	I
12	Complex landslide	759	662	304,123	3,102,055	V
13	Complex landslide	779	443	212,055	2,162,961	IV
14	Complex landslide	620	339	149,805	1,528,011	V
15	Complex landslide	362	179	35,235	359,397	VI

Note. Length, width, and area have been estimated from the geomorphological map. Volume estimates are total net gain proportional to RSF area, involving an average thickness of approximately 10 m for RSF bodies. The relative age sequence proposed is based on cross-cutting and superimposition relationships between RSFs, topographic preservation of RSFs, and differences in the vegetation coverage.

4.2. Sedimentary records from impounded floodplains

Sediment cores Canamora-01 and Canamora-02 were drilled into two floodplains placed upstream from RSFs deposits (Figure 6). Canamora-01 (UTM coordinates: 303827X–4771015Y; 1356 m asl; 3.06-m depth) contains alternations of grey to dark brown clay sediments massive or laminated, with gravel intervals with sandy and muddy matrix. Gravel intervals correspond to shale and sandstone fragments with particle sizes up to 1.6 cm in diameter (0.5 cm in the lowest interval) and subangular to subrounded shape, evidencing a water transport (Figure 7). Similarly, Canamora-02 (UTM coordinates: 303020X–4770968Y; 1325 m asl; 4.02-m depth) contains alternations of grey to dark brown clay sediments, frequently laminated, with intervals of massive gravel sediments with sandy matrix. Gravel intervals are dominant in the lowest approximately 1.5 m of the sequence and show subrounded to rounded sandstone and mudstone fragments up to 4 cm in diameter (Figure 7). Following the lithofacies classification in Miall (1985), the laminated to massive mud intervals are identified as back swamp deposits (Fsc); gravel intervals as sieved deposits (Gm); and the initial 60 cm in both cores correspond to seat-earth or soil (Fr). The stacking of lithofacies associations Gm and Fsc observed in both cores is interpreted as the consequence of a fast abandonment of the bed load (Gm facies) followed by decantation of the suspended load (Fsc facies) due to a sudden blockage of the valley caused by an RSF event. Up to three episodes of floodplain aggradation have been identified in each core in response to RSFs. In Canamora-01, sequence aggradation episodes would be explained by RSFs 11, 4 and 10, whereas in Canamora-02, they would be mostly related to RSFs 2 and 12. Table 2 compiles radiocarbon results and calibrated ages for five samples corresponding to plant macro remain or bulk sediment (laminated clay) taken from both sediment cores in the different aggradation sequences. A minimum age of 13130 ± 100 ^{14}C years was obtained for the lowest Fsc interval in the Canamora-01 sequence related to valley blockage by RSF 11 (16062–15369 cal years BP). However, the bulk sediment sample analyzed in the Fsc interval above displays significantly younger result of 3910 ± 35 ^{14}C years (4429–4239 cal years BP) and could correspond to RSF 4. Finally, the age provided for a plant remain sample from the base of the last Gm interval revealed an age of 1720 ± 30 ^{14}C (1702–1559 cal years BP) and would be linked to RSF 10. In contrast, the closest to the base sample analyzed in Canamora-02 core corresponded to wood remains that yielded a minimum age of 3295 ± 30 ^{14}C years (3586–3452 cal years BP) for RSF 2, whereas the Gm interval placed on top provided a result of 3170 ± 30 ^{14}C years (3452–3346 cal years BP) and is attributed to RSF 12. Considering the present year (instead 1950) to compare radiocarbon ages with surface exposure ages obtained in the local glacial record and estimate post-glacial denudation rates, the minimum age of valley impoundment due to paraglacial slope instabilities in the San

Isidro valley lies in the range 16.1–15.4 ka for the Canamora-01 floodplain, while it is in the range 3.6–3.5 ka in the case of the Canamora-02 floodplain.

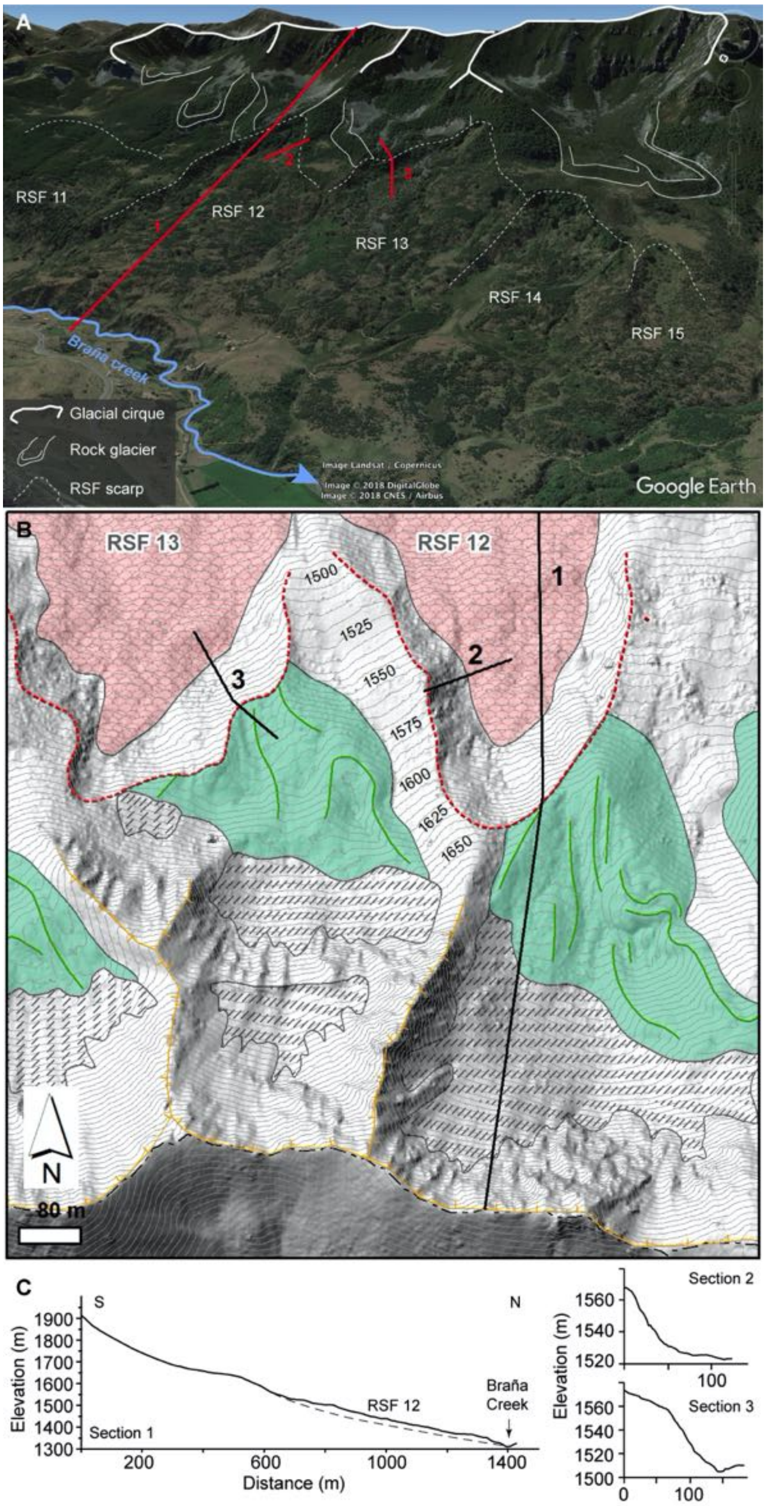

Figure 5.- (a) Google Earth view of the northern slope of the Fuentes de Invierno range showing the location of glacial cirque headwalls and the cross-cut relationships between the toe of rock glaciers and the scarps of subsequent rock-slope failures (RSFs). (b) Detailed view of the geomorphological map (see legend in figure 3) showing the crest zone of the Fuentes de Invierno range and the spatial relationship between glacial cirques, rock glaciers, and the source area of RSFs 12 and 13. (c) Section 1 shows the long-profile of RSF 12 from the crest zone of the Fuentes de Invierno range to the valley bottom. Sections 2 and 3 correspond to close-up profiles of the scarps of RSFs 12 and RSF 13, which clearly interrupt the ridge-trough topography of rock glaciers.

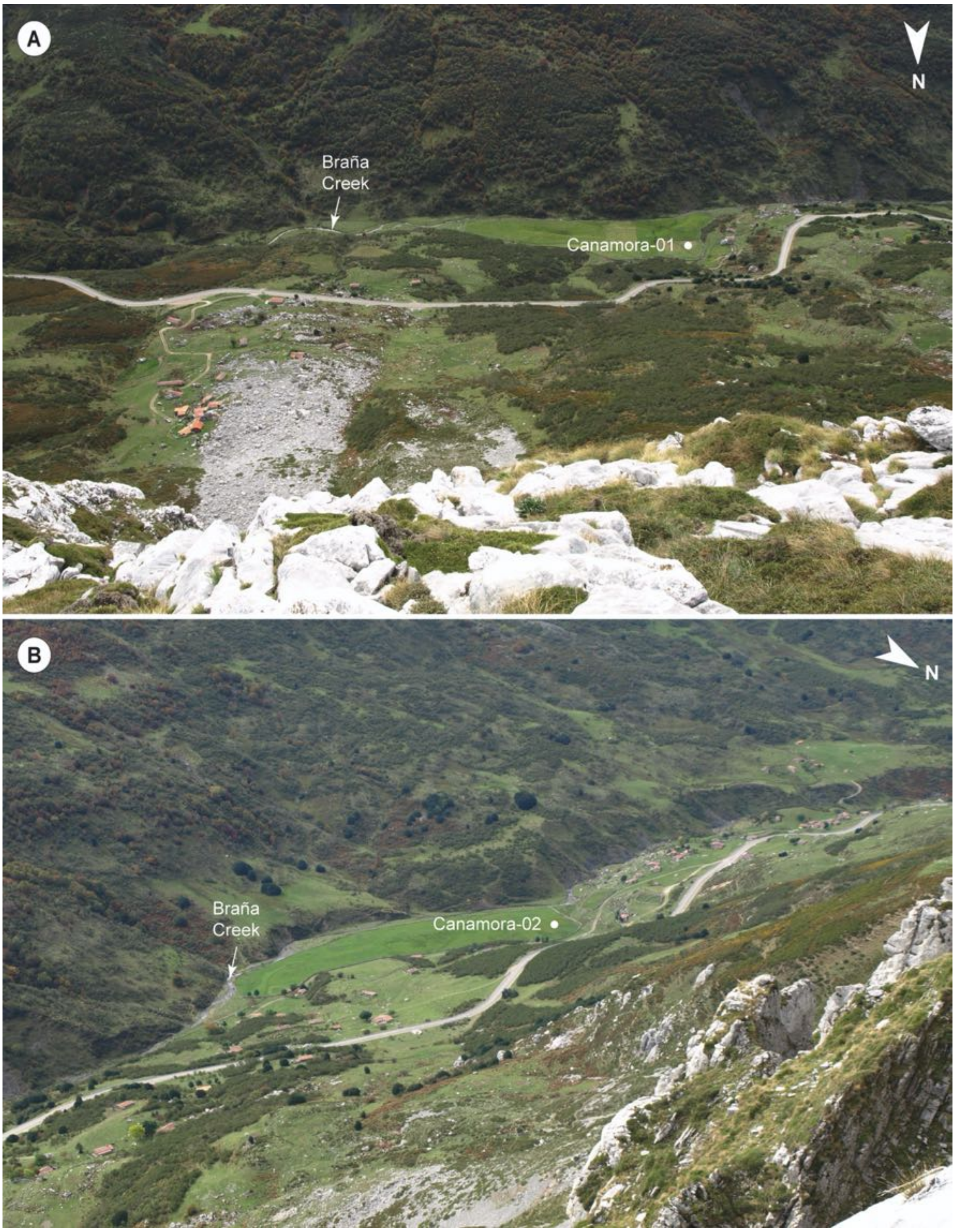

Figure 6.- Sediment core extraction in two floodplains deposited upstream from RSFs deposits (core locations are shown in Figure 3): (a) Canamora-01; and (b) Canamora-02.

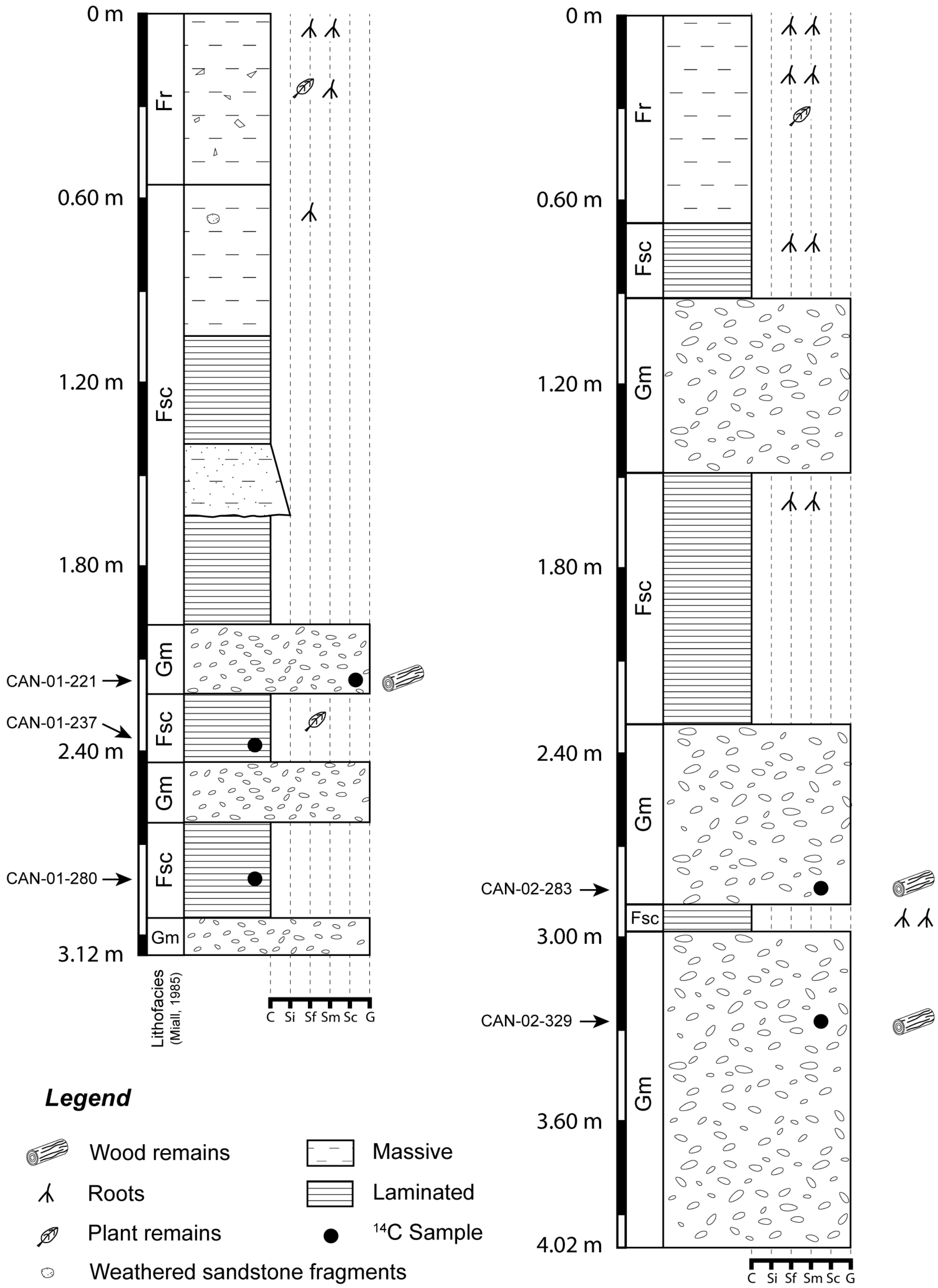

Figure 7.- Stratigraphic columns of Canamora-01 and Canamora-02 sediment cores (C, clay; Si, silt; Sf, fine sand; Sm, medium sand; Sc, coarse sand; G, gravel). Core locations are shown in Figure 3.

Table 2. Radiocarbon samples from the Canamora sediment cores drilled in the floodplains of the San Isidro valley (central Cantabrian Mountains).

Reference	Depth (cm)	Laboratory reference	Sampled material	C-14 age (years BP)	Calibrated age (Years BP 2 sigma)
CAN-01-221	221	Poz-75605	Plant macro remains	1720 ± 30	1559 – 1702
CAN-01-237	237	Poz-75606	Bulk sediment	3910 ± 35	4239 – 4429
CAN-01-280	280	Poz-75786	Bulk sediment	13130 ± 100	15369 – 16062
CAN-02-283	283	Poz-75415	Plant macro remains	3170 ± 30	3346 – 3452
CAN-02-329	329	Poz-75284	Plant macro remains	3295 ± 30	3452 – 3586

Note. Radiocarbon ages calibrated with Calib Rev 7.0.2 program (Stuiver and Reimer, 1993) and the IntCal13 curve (Reimer et al., 2013).

4.3. Quantification of post-glacial erosion rates

A topographic restitution of the San Isidro valley prior to the occurrence of RSFs allowed the original U-shaped section of the valley to be restored (Figure 8). The DEM analysis revealed that a total volume of 29.2 Mm^3 of hard rock material was removed from the valley sides due to paraglacial RSFs. However, the net volume of sediments gained at the hillslope foot is 22.4 Mm^3, which is lower than expected most likely due to subsequent fluvial erosion. Hard rock crushes and expands during a RSF event, so the expected volume deficit ascribable to fluvial erosion of RSF toe areas should be greater than 6.8 Mm^3 (difference between net volume losses and gains). In order to estimate the volume removal ascribable to fluvial down-cutting of RSF toe areas, we applied several expansion coefficients (expressed as percent of porosity increase) to the net volume loss of hard rock material to infer the initial volume occupied by RSF sediments (Table 3). Differences between the inferred initial volume and the actual volume of RSF bodies provide an estimate of material eroded from RSF areas due to post-depositional fluvial erosion. A previous study on porosity measurements of soils developed on shallow landslides have shown values in the range 1-15% (Table ST2 of the supplementary material included in Bogner et al. (2014). Assuming a porosity increase of 5%, 10%, 15% and 20% compared to the original volume of rock material, paraglacial RSF bodies would have involved a total volume of 30.7 to 35.1 Mm^3 due to crushing during transport. Taking a porosity increase range of 10 to 15% as the most probable, the volume of RSF materials removed by fluvial erosion would be 11.2 to 9.7 Mm^3. If this volume loss is normalized to the area affected by RSFs (approximately 3.13 Mm^2), fluvial erosion would have been responsible for a surface lowering of 3.6 to 3.1 m. Thus, a fluvial erosion rate of 0.19–0.22 mm a^{-1} is estimated based on the inferred amount of surface lowering and assuming a minimum reference age of approximately 16.1 ka for RSFs (Table 3). The erosion rate would decrease down to 0.05 mm a^{-1} when the volume loss is normalized to the basin area. This decrease is because fluvial erosion of RSF materials represents just part of the total fluvial erosion affecting the study basin. Moreover, fluvial erosion rates normalized-to-area assume a uniform lowering for the surface extent considered. However, erosion rates are higher along the main channel. Fluvial erosion rates of 7.6 ± 1.2 mm a^{-1} were estimated along the Braña Creek using the ratio between the height of fluvial scarps at the toe of RSF 2 (27 ± 5 m) and the oldest minimum age available of approximately 3.6 ka. Also, fluvial erosion rates derived upstream from other erosive scarps cutting both sediments and bedrock (37 ± 12 m) provide erosion rates in the range 2.5 ± 0.8 and 2.2 ± 0.7 mm a^{-1} assuming that last deglaciation occurred at least 17–15 ka ago (Rodríguez-Rodríguez et al., 2016)

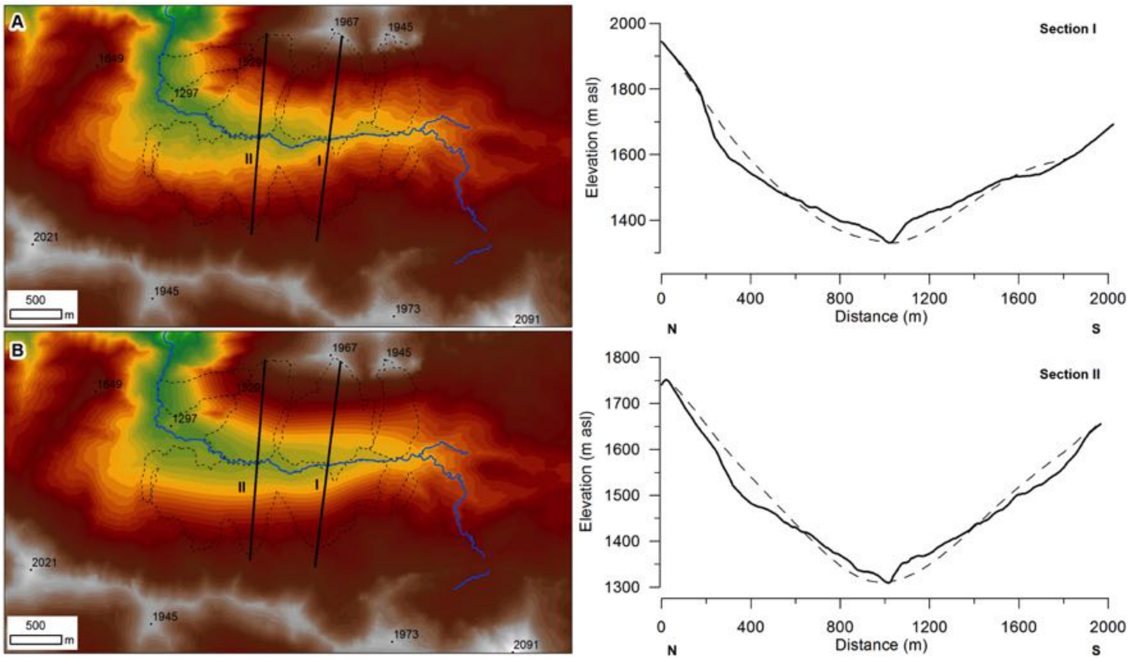

Figure 8.- Comparison between the digital elevation model at present (a) and (b) prior to rock-slope failure (RSF) occurrence approximately prior to 16.1 ka (10-m cell-size resolution; 20-m intervals). Dashed lines represent the area affected by RSFs. Topographic sections show changes in the San Isidro cross-section before (dashed line) and after (solid line) paraglacial RSFs.

Table 3. Estimate of total volume initially occupied by RSFs in the San Isidro valley applying different porosity increases to the net volume loss of rock materials at the highest portion of the hillslopes.

Porosity increase (%)	**RSF volume (m^3)**		**Erosion of total RSF area (depth eq. in m)**	**Rate ($mm\ a^{-1}$)**	**Erosion of basin area (depth eq. in m)**	**Rate ($mm\ a^{-1}$)**
5	30688943	Initial	2.64	0.16	0.63	0.04
	8271442	Eroded				
10	32150321	Initial	3.11	0.19	0.74	0.05
	9732820	Eroded				
15	33611700	Initial	3.58	0.22	0.86	0.05
	11194198	Eroded				
20	35073078	Initial	4.04	0.25	0.97	0.06
	12655577	Eroded				

Note. Subsequent volume loss due to fluvial erosion was calculated as the difference between the initial volume and the actual volume calculated for the RSF bodies. Volume losses were normalized to the area affected by RSFs and to the 2D area of the study basin, allowing the calculation of normalized erosion rates (expressed as depth equivalent in meters).

5. Discussion

5.1. Timing of RSFs and factors involved

The combination of local bedrock geology (pre-conditioning factor) and glacial modeling (preparatory/triggering factor) resulted in a clustering of RSFs that have greatly modified the topography of the San Isidro valley, masking the original parabolic shaped cross-section. The last deglaciation was followed by a series of RSFs that continue throughout the Holocene, affecting both hillslopes and causing recurrent episodes of valley blockage and floodplain aggradation. A relative age sequence for RSF events was established based on the spatial analysis of landform assemblages and complemented with the study of related floodplain sequences. Preliminary radiocarbon dates are consistent with the relative age sequence proposed, suggesting a minimum age of 16.1 ka for the oldest RSFs that promoted the deposition of Canamora-01 sequence. This result is consistent with the end of last deglaciation and coeval with rock glacier activity in the highest areas of Fuentes de Invierno Range. This is supported by ^{10}Be surface exposure ages reported in the adjacent Porma basin, which indicate glacier retreat conditions by 17.7 ± 0.4 ka and rock glacier fronts at 1620 m asl stable by 15.7 ± 0.3 ka (Rodríguez-Rodríguez et al., 2016). Similarly, minimum ^{10}Be surface exposure ages recently reported for the nearby Monasterio valley (approximately 6 km to the East) suggest that glaciers were restricted to the cirques by 14 ± 0.3 ka and rock glacier fronts were stabilized at 1540 m asl around 13 ± 0.2 ka ago (Rodríguez-Rodríguez et al., 2017). Because rock glaciers preserved in the south hillslope of the San Isidro valley have their frontal ridges placed at similar altitudes (1520–1700 m asl), their stabilization ages are expected to be comparable to those reported in the Porma and Monasterio valleys (figure 1). Additionally, this RSF episode also matches cold and dry climate conditions identified in a stalagmite record from El Pindal Cave between 18.2 and 15.4 ka (Moreno, Stoll, et al., 2010). Given that

RSFs linked to basal Canamora-01 sequence occurred shortly after deglaciation, glacial erosion and debuttressing could either have acted as triggering factors or, at least, have played a significant role as conditioning/preparatory factors. The nearly vertical dip angle of bedding planes in both flanks of the San Isidro Antiform (Figure 1), oriented parallel to the valley direction, together with the alternation of hard and soft lithologies (both pre-conditioning factors) might have favored the opening of bedding discontinuities and joints under glacial debuttressing and stress release conditions (preparatory/trigger factors). In such scenario, periglacial freeze-thaw cycles and soil water saturation conditions (linked to meltdown) could have had a role as triggers. Subsequent RSF events at approximately 4.5 ka (rock avalanche) and 1.8 ka (small complex landslide) also blocked the valley, causing new episodes of floodplain impoundment and sediment aggradation.

In contrast, the oldest ages obtained in Canamora-02 sequence suggest that floodplain sedimentation started later, due to an RSF event that occurred around 3.6 ka. This event was probably a rock avalanche affecting the northern hillslope that forced the stream to migrate southwards, undercutting the southern hillslope and promoting other RSFs in the southern slope that clearly cut the frontal ridges of relict rock glaciers. The lag-time or pre-failure endurance between RSFs responsible for valley impoundment and floodplain aggradation is approximately 12 ka, suggesting that glacier-induced changes in the hillslopes have constituted key preparatory factors for all RSFs, but have not necessarily acted as triggering factors. At a first glance, the high spatial density of RSFs in the San Isidro valley could be compatible with a seismic origin as it has been previously documented in other regions like China or India (Xu, Zhang, & Li, 2011; Yuan et al., 2013). Historic earthquakes recorded in northwest Iberia mostly occurred in an area known as the Becerreá Swarm, located far West (approximately 140 km) from San Isidro valley, and showed Mw < 5.1 (Llana-Fúnez & López-Fernández, 2015). In the province of Asturias, the most intense historic event was recorded at Teverga (-6.000, 43.330) in 1950 and corresponded to a Mw of 4.6 (http://www.ign.es/web/ign/portal/terremotos-importantes; last access on December 2017). The Teverga earthquake, occurred approximately 55 km west from San Isidro, would be within the minimum earthquake magnitude of $M_w = 4.3 \pm 0.4$ required to generate coseismic landslides (Malamud, Turcotte, Guzzetti, & Reichenbach, 2004). Although strong earthquakes have been rare in the historic record, it would be expected that higher magnitude events might have occurred over the last 16 ka, leaving open the possibility of a seismic trigger for some of these landslides.

Despite the possibility of seismic triggers, we favor the idea that climate/rainfall is responsible for the increase RSF activity at 4.5 ka. Pollen records from the NW Cantabrian Mountains suggest a woodland expansion phase at 4.0–2.5 ka that would be consistent with wetter climate conditions (Muñoz-Sobrino, Ramil-Rego, Gómez-Orellana, & Díaz-Varela, 2005). The sedimentary sequence of Enol Lake in Picos de Europa (the highest mountain massif of the Cantabrian Mountains) also indicates wet conditions at 4.6–2.2 ka (Moreno, Valero-Garcés, et al., 2010). In the same area, peat bogs formed at Vega de Comeya during the time interval 6.3–3.1 ka (Urbańczyk, Bechtel, & Borrego, 2016). All these continental archives indicate that part of the Holocene RSFs sequence occurred during a wet climate period, pointing to rainfall as the most likely triggering factor or preparatory factor if the rainfall induced enhanced fluvial incision rather than triggered the slope failures directly. Mid-Holocene RSFs may have been triggered by increased fluvial incision and/or elevated pore water pressure due to high river flow discharge under wetter climate conditions. Also, the occurrence of RSF events might have contributed as well to create forced river incision along landslide occlusions and increase pore water pressure in the hillslopes placed upstream due to valley impoundment. The Mid-Holocene RSF events documented are time consistent with landslides occurring at 3–5 ka in the Pas river basin (Cantabria province to the East in nonparaglacial context), where no direct evidence for triggering factors has been found but rainfall was assumed the most likely one (González-Díez, Remondo, Díaz de Terán, & Cendrero, 1999). The analysis of press archives as temporal records of modern landslide events in Asturias suggest the importance of rainfall events on landslide triggering (Domínguez-Cuesta, Jiménez-Sánchez, & Rodríguez-García, 1999). A broader study in the same region has shown that landslide events mainly occur once soil moisture condition has reached critical saturation value, with 98% of events occurring under available water capacity levels of 99-100% (Valenzuela, Domínguez-Cuesta, Mora-García, & Jiménez-Sánchez, 2018). Under water-saturated soil conditions, the hydraulic pressure reduces friction and favors slope failure. In an European context, a previous study on deep-seated landslides in a non-glaciated area of the Southern Alps reported cosmic ray exposure ages of 3.3 to 5.1 ka, and consider them as climatically driven by the 4.2 ka event, the heaviest rainfall period of the entire Holocene (Zerathe, Lebourg, Braucher, & Bourlès, 2014).

5.2. Denudation signature

Apatite fission track studies indicate that the main period of exhumation of the Cantabrian Mountains at its Western end began in the Palaeogene at rates of 0.02 mm a^{-1} and continued during the Neogene at rates of approximately 0.06 mm a^{-1} (Martín-González, Barbero, Capote, Heredia, & Gallastegui, 2012). Tectonic uplift rates based on geomorphological indicators in the Western end of the Cantabrian Mountains gave estimates of 0.10 mm a^{-1} over the past 600 ka based on the Miño river terraces (Viveen et al., 2014). An eastward rising trend in tectonic uplift has been suggested on the basis of marine terrace exposure time analysis, with values ranging from 0.07 to 0.15 mm a^{-1} for the last 1–2 Ma (Álvarez-Marrón et al., 2008). Incision rates of 0.1 to 0.3 mm a^{-1} were estimated in the central Cantabrian Mountains based on perched phreatic conduits in caves connected to the Urdon gorge from Picos de Europa (Smart, 1986). Ruíz-Fernández and Poblete-Piedrabuena (2011) calculated a rate of 0.24 mm a^{-1} on the basis of fluvial terraces of the Cares river that drains the Picos de Europa massif. Farther north, a rate of 0.19 mm a^{-1} was calculated based on minimum ages derived from U-Th dating of speleothems at El Pindal Cave in the Cantabrian Coast (Jiménez-Sánchez et al., 2006). The incision rates of 2.5–2.2 mm a^{-1} derived from gullies carved on shale bedrock in the study area since the retreat of glaciers are an order of magnitude higher than previous estimates and suggest significant acceleration of fluvial incision rates since the last deglaciation.

The DEM analysis in San Isidro shows that paraglacial RSFs have eroded approximately 29.2 Mm^3 of hard rock from the upper part of hillslopes, inducing dramatic changes in surface topography and easing fluvial erosion processes. The fluvial erosion rate estimated for the area affected by RSFs is 0.2 mm a^{-1} over the last 16.1 ka, a value that seems consistent compared to previous incision rate estimates in the central Cantabrian Mountains. However, this is a normalized rate calculated assuming a uniform lowering for the entire area affected by RSFs, which is an unrealistic scenario given the fact that fluvial incision concentrates along the foot areas of RSF occlusions (as evidenced by the presence of fluvial scarps in the foots of most RSFs). The incision value inferred for the San Isidro valley at the toe of RSF 2 is approximately 7.6 mm a^{-1}, almost three times higher than incision rates of 2.5–2.2 mm a^{-1} derived from local gullies upstream. This result demonstrates that paraglacial instabilities contribute to accelerate fluvial incision rates when their deposits are coupled with streams, ensuring an efficient sediment transfer (Cossart et al., 2013).

6. Conclusions

A series of RSFs occurred in the San Isidro valley after the last deglaciation, reaching the valley bottom and causing river damming and floodplain sedimentation. The analysis of spatial relationships between the different types of RSFs and the sedimentary records of two related floodplains suggest a long history of recurrent RSF events and floodplain aggradation. Several episodes of RSF damming and aggradation were identified in the floodplain sequences and dated with radiocarbon, suggesting that RSFs started early after local deglaciation (approximately 16.1 ka) and spanned the entire Holocene with some identified events at ca. 4.5, 3.6–3.5, and 1.8 ka. Although further chronological studies are required to better constrain variations in RSF frequency between the Lateglacial and the Holocene, preliminary results reassure the idea that paraglacial RSF activity may span several millennia. Whereas glacial debuttressing and stress release conditions following glacier retreat played a key role in hillslope destabilization during the oldest events, mid-Holocene RSFs were most likely triggered by an increase in rainfall frequency (related to the 4.2 ka event) and enhanced fluvial down-cutting of valley hillslopes. Thus, ultimate triggering factors related to RSFs may vary through time. Future studies in the area should focus on geting more datable material from impounded floodplain sections and also the application of cosmogenic isotope analysis of limestone boulders in rock avalanches.

The quantification of fluvial incision rates in the study area and its comparison to previous estimates based in other geomorphological proxies suggests a significant rise in fluvial incision since the last deglaciation. Another interesting finding is that we have quantified that the occurrence of RSFs significantly contributed to rise fluvial incision, multiplying by a factor of three the local incision rates. This in turn demonstrates the capacity of RSFs in causing an accelerated degradation of the landscape when they are coupled with fluvial processes.

Acknowledgements

Research funded by Ministerio de Industria, Economía y Competitividad (MINECO) of Gobierno de ESpaña and the European Regional Development Fund (CANDELA project, reference CGL2012-31938). Additional funding provided by Gobierno del Principado de Asturias (PCTI) and the European Regional Development Fund (GEOCANTABRICA research group, reference FC-15-GRUPIN14-044). Laura Rodríguez is grant holder of the Marie Curie–Clarín COFUND program financed jointly by Gobierno del Principado de Asturias and the 7th WP of the European Union / Marie Curie Actions (Reference ACA-17-19). This is a contribution of the GEOCANTABRICA and GeoQUO research groups. We are grateful to Jasper Knight, Tomáš Pánek, and two anonymous reviewers as well as to editor Samuel T. McColl for their helpful comments and suggestions that greatly improved the original version of this paper.

References

Alonso, J. L., Marcos, A., & Suárez, A. (2009). Paleogeographic inversion resulting from large out of sequence breaching thrusts: The León Faults (Cantabrian Zone, NW Iberia). A new picture of the external Variscan Thrust Belt in the Ibero-Armorican Arc. *Geologica Acta, 7*(4), 451-473. doi:10.1344/105.000001449

Alonso, J. L., Pulgar, J. A., García-Ramos, J. C., & Barba, P. (1996). Tertiary basins and Alpine tectonics in the Cantabrian Mountains (NW Spain). In P. Friend & C. Dabrios (Eds.), *Tertiary basins of Spain: the stratigraphic record of crustal kinematics* (pp. 214-227). Cambridge: Cambridge University Press.

Álvarez-Marrón, J., Heredia, N., & Pérez-Estaún, A. (1989). Mapa geológico de la Región del Ponga. *Trabajos de geología, 18*, 127-135.

Álvarez-Marrón, J., Hetzel, R., Niedermann, S., Menéndez, R., & Marquínez, J. (2008). Origin, structure and exposure history of a wave-cut platform more than 1 Ma in age at the coast of northern Spain: A multiple cosmogenic nuclide approach. *Geomorphology, 93*(3-4), 316-334. doi:10.1016/j.geomorph.2007.03.005

Ballantyne, C. K. (2002). Paraglacial geomorphology. *Quaternary Science Reviews, 21*, 1935-2017. doi:10.1016/S0277-3791(02)00005-7

Ballantyne, C. K., Sandeman, G. F., Stone, J. O., & Wilson, P. (2014). Rock-slope failure following Late Pleistocene deglaciation on tectonically stable mountainous terrain. *Quaternary Science Reviews, 86*, 144-157. doi:10.1016/j.quascirev.2013.12.021

Ballantyne, C. K., & Stone, J. O. (2013). Timing and periodicity of paraglacial rock-slope failures in the Scottish Highlands. *Geomorphology, 186*, 150-161. doi:10.1016/j.geomorph.2012.12.030

Bogner, C., Bauer, F., Trancón y Widemann, B., Viñan, P., Balcazar, L., & Huwe, B. (2014). Quantifying the morphology of flow patterns in landslide-affected and unaffected soils. *Journal of Hydrology, 511*, 460-473. doi:10.1016/j.jhydrol.2014.01.063

Cossart, E., Braucher, R., Fort, M., Bourlès, D. L., & Carcaillet, J. (2008). Slope instability in relation to glacial debuttressing in alpine areas (Upper Durance catchment, southeastern France): Evidence from field data and ^{10}Be cosmic ray exposure ages. *Geomorphology, 95*(1-2), 3-26. doi:10.1016/j.geomorph.2006.12.022

Cossart, E., Mercier, D., Decaulne, A., & Feuillet, T. (2013). An overview of the consequences of paraglacial landsliding on deglaciated mountain slopes: typology, timing and contribution to cascading fluxes. *Quaternarie, 24*(1), 13-24. doi:10.4000/quaternaire.6444

Dadson, S. J., & Church, M. (2005). Postglacial topographic evolution of glaciated valleys: a stochastic landscape evolution model. *Earth Surface Processes and Landforms, 30*(11), 1387-1403. doi:10.1002/esp.1199

Domínguez-Cuesta, M. J., Jiménez-Sánchez, M., & Rodríguez-García, A. (1999). Press archives as temporal records of landslides in the North of Spain: relationships between rainfall and instability slope events. *Geomorphology, 30*, 125-132. doi:10.1016/S0169-555X(99)00049-5

García-Couto, M. A. (Ed.) (2011). *Iberian Climate Atlas*. Madrid: Agencia Estatal de Meteorología (AEMET) and Instituto de Meteorología de Portugal (IM).

Gómez-Villar, A., González-Gutiérrez, R. B., Redondo-Vega, J. M., & Santos-González, J. (2011). Distribución de glaciares rocosos relictos en la Cordillera Cantábrica. *Cuadernos de Investigación Geográfica, 37*(2), 49-80.

González-Díez, A., Remondo, J., Díaz de Terán, J. R., & Cendrero, A. (1999). A methodological approach for the analysis of the temporal occurrence and triggering factors of landslides. *Geomorphology, 30*, 95-113. doi:10.1016/S0169-555X(99)00047-1

Ivy-Ochs, S., Kerschner, H., Reuther, A., Preusser, F., Heine, K., Maisch, M., . . . Schlüchter, C. (2008). Chronology of the last glacial cycle in the European Alps. *Journal of Quaternary Science, 23*(6-7), 559-573. doi:10.1002/jqs.1202

Jarman, D., Calvet, M., Corominas, J., Delmas, M., & Gunnell, Y. (2016). Large-scale rock slope failures in the eastern pyrenees: identifying a sparse but significant population in paraglacial and parafluvial contexts. *Geografiska Annaler: Series A, Physical Geography, 96*(3), 357-391. doi:10.1111/geoa.12060

Jiménez-Sánchez, M., Bischoff, J. L., Stoll, H., & Aranburu, A. (2006). A geochronological approach for cave evolution in the Cantabrian Coast (Pindal Cave, NW Spain). *Zeitschrift fur Geomorphologie N.F., 147*, 129-141.

Julivert, M. (1971). Decollement tectonics in the Hercynian Cordillera of Northwestern Spain. *American Journal of Science, 270*, 1-29. doi:10.2475/ajs.270.1.1

Kellerer-Pirklbauer, A., Proske, H., & Strasser, V. (2010). Paraglacial slope adjustment since the end of the Last Glacial Maximum and its long-lasting effects on secondary mass wasting processes: Hauser Kaibling, Austria. *Geomorphology, 120*(1-2), 65-76. doi:10.1016/j.geomorph.2009.09.016

Lebourg, T., Zerathe, S., Fabre, R., Giuliano, J., & Vidal, M. (2014). A Late Holocene deep-seated landslide in the northern French Pyrenees. *Geomorphology, 208*, 1-10. doi:10.1016/j.geomorph.2013.11.008

Llana-Fúnez, S., & López-Fernández, C. (2015). The seismogenic zone of the continental crust in Northwest Iberia and its relation to crustal structure. *Tectonics, 34*, 1751-1767. doi:10.1002/2015TC003877

Malamud, B. D., Turcotte, D. L., Guzzetti, F., & Reichenbach, P. (2004). Landslides, earthquakes, and erosion. *Earth and Planetary Science Letters, 229*(1-2), 45-59. doi:10.1016/j.epsl.2004.10.018

Marquínez, J. (1992). *Tectónica y relieve en la cornisa cantábrica.* Paper presented at the The Late Quaternary in the western Pyrenean region.

Martín-González, F., Barbero, L., Capote, R., Heredia, N., & Gallastegui, G. (2012). Interaction of two successive Alpine deformation fronts: constraints from low-temperature thermochronology and structural mapping (NW Iberian Peninsula). *International Journal of Earth Sciences, 101*(5), 1331-1342. doi:10.1007/s00531-011-0712-9

McColl, S. T. (2012). Paraglacial rock-slope stability. *Geomorphology, 153-154*, 1-16. doi:10.1016/j.geomorph.2012.02.015

Mercier, D., Coquin, J., Feuillet, T., Decaulne, A., Cossart, E., Jónsson, H. P., & Sæmundsson, Þ. (2017). Are Icelandic rock-slope failures paraglacial? Age evaluation of seventeen rock-slope failures in the Skagafjörður area, based on geomorphological stacking, radiocarbon dating and tephrochronology. *Geomorphology, 296*, 45-58. doi:10.1016/j.geomorph.2017.08.011

Miall, A. D. (1985). Architectural-Element Analysis: A new method of facies analysis applied to fluvial deposits. *Earth-Science Reviews, 22*, 261-308.

Moreno, A., Stoll, H., Jiménez-Sánchez, M., Cacho, I., Valero-Garcés, B., Ito, E., & Edwards, R. L. (2010). A speleothem record of glacial (25–11.6kyr BP) rapid climatic changes from northern Iberian Peninsula. *Global and Planetary Change, 71*(3-4), 218-231. doi:10.1016/j.gloplacha.2009.10.002

Moreno, A., Valero-Garcés, B. L., Jiménez-Sánchez, M., Domínguez-Cuesta, M. J., Mata, M. P., Navas, A., . . . Rico, M. (2010). The last deglaciation in the Picos de Europa National Park (Cantabrian Mountains, northern Spain). *Journal of Quaternary Science, 25*(7), 1076-1091. doi:10.1002/jqs.1265

Muñoz-Sobrino, C., Ramil-Rego, P., Gómez-Orellana, L., & Díaz-Varela, R. (2005). Palynological data on major Holocene climatic events in NW Iberia. *Boreas, 34*(3), 381-400. doi:10.1080/03009480510013006

Nagelisen, J., Moore, J. R., Vockenhuber, C., & Ivy-Ochs, S. (2015). Post-glacial rock avalanches in the Obersee Valley, Glarner Alps, Switzerland. *Geomorphology, 238*, 94-111. doi:10.1016/j.geomorph.2015.02.031

Pánek, T., Engel, Z., Mentlík, P., Braucher, R., Břežný, M., Škarpich, V., & Zondervan, A. (2016). Cosmogenic age constraints on post-LGM catastrophic rock slope failures in the Tatra Mountains (Western Carpathians). *Catena, 138*, 52-67. doi:10.1016/j.catena.2015.11.005

Pérez-Estaún, A., Bastida, F., Alonso, J. L., Marquínez, J., Aller, J., Álvarez-Marrón, J., . . . Pulgar, J. A. (1988). A thin-skinned tectonics model for an arcuate fold and thrust belt: The Cantabrian Zone (Variscan Ibero-Armorican Arc). *Tectonics, 7*, 517-537. doi:10.1029/TC007i003p00517

Pulgar, J. A., Gallart, J., Fernández-Viejo, G., Pérez-Estaún, A., Álvarez-Marrón, J., & Group, E. (1996). Seismic image of the Cantabrian Mountains in the western extension of the Pyrenees from integrated ESCIN reflection and refraction data. *Tectonophysics, 264*, 1-19. doi:10.1016/S0040-1951(96)00114-X

Reimer, P., Bard, E., Bayliss, A., Beck, J. W., Blackwell, P., Ramsey, C. B., . . . van der Plicht, J. (2013). Intcal13 and Marine13 radiocarbon age calibration curves 0-50,000 years cal BP. *Radiocarbon, 55*(4), 1869-1887. doi:10.2458/azu_js_rc.55.16947

Rodríguez-Pérez, C. (1995). Estudio geomorfológico del puerto de San Isidro. *Eria, 36*, 63-87.

Rodríguez-Rodríguez, L. (2015). *Quaternary Glaciations in the Central Cantabrian Mountains: new geomorphological and geochronological contributions.* (PhD thesis), University of Oviedo.

Rodríguez-Rodríguez, L., Jiménez-Sánchez, M., Domínguez-Cuesta, M. J., Rinterknecht, V., Pallàs, R., Aumaître, G., . . . Keddadouche, K. (2017). Timing of last deglaciation in the Cantabrian Mountains (Iberian Peninsula; North Atlantic Region) based on in situ-produced ^{10}Be exposure dating. *Quaternary Science Reviews, 171*, 166-181. doi:10.1016/j.quascirev.2017.07.012

Rodríguez-Rodríguez, L., Jiménez-Sánchez, M., Domínguez-Cuesta, M. J., Rinterknecht, V., Pallàs, R., & Bourlès, D. (2016). Chronology of glaciations in the Cantabrian Mountains (NW Iberia) during the Last Glacial Cycle based on in situ-produced ^{10}Be. *Quaternary Science Reviews, 138*, 31-48. doi:10.1016/j.quascirev.2016.02.027

Ruíz-Fernández, J., & Poblete-Piedrabuena, M. A. (2011). Las terrazas fluviales del río Cares: aportaciones sedimentológicas y cronológicas (Picos de Europa, Asturias). *Estudios geográficos, 72*(270), 173-202. doi:10.3989/estgeogr.201108

Slaymaker, O. (2011). Criteria to Distinguish Between Periglacial, Proglacial and Paraglacial Environments. *Quaestiones Geographicae, 30*(1). doi:10.2478/v10117-011-0008-y

Smart, P. L. (1986). Origin and development of glacio-karst closed depressions in the Picos de Europa, Spain. *Zeitschrift fur Geomorphologie N.F., 30*(4), 423-443.

Southall, D. W., Wilson, P., Dunlop, P., Schnabel, C., Rodés, A., Gulliver, P., & Xu, S. (2017). Age evaluation and causation of rock-slope failures along the western margin of the Antrim Lava Group (ALG), Northern Ireland, based on cosmogenic isotope (36Cl) surface exposure dating. *Geomorphology, 285*, 235-246. doi:10.1016/j.geomorph.2017.01.041

Stuiver, M., & Reimer, P. J. (1993). Extended ^{14}C data base and revised CALIB 3.0 ^{14}C age calibration program. *Radiocarbon, 35*, 215-230. doi:10.1017/S0033822200013904

Suárez-Rodríguez, A. (1987). Mapa geomorfológico 1:50,000, Hoja nº 79 (Puebla de Lillo). In IGME (Ed.), *Serie MAGNA*. Madrid.

Urbańczyk, J., Bechtel, A., & Borrego, A. G. (2016). Organic geochemical evidence of postglacial paleoenvironmental evolution of the Comeya peatland (Asturias, N Spain). *International Journal of Coal Geology, 168*, 46-54. doi:10.1016/j.coal.2016.10.001

Valenzuela, P., Domínguez-Cuesta, M. J., Mora-García, M. A., & Jiménez-Sánchez, M. (2018). Rainfall thresholds for the triggering of landslides considering previous soil moisture conditions (Asturias, NW Spain). *Landslides, 15*(2), 273-282. doi:10.1007/s10346-017-0878-8

Vehling, L., Baewert, H., Glira, P., Moser, M., Rohn, J., & Morche, D. (2017). Quantification of sediment transport by rockfall and rockslide processes on a proglacial rock slope (Kaunertal, Austria). *Geomorphology, 287*, 46-57. doi:10.1016/j.geomorph.2016.10.032

Viveen, W., Schoorl, J. M., Veldkamp, A., & van Balen, R. T. (2014). Modelling the impact of regional uplift and local tectonics on fluvial terrace preservation. *Geomorphology, 210*, 119-135. doi:10.1016/j.geomorph.2013.12.026

Whipple, K. X., Kirby, E., & Brocklehurst, S. H. (1999). Geomorphic limits to climate-induced increases in topographic relief. *Nature, 401*, 39-43. doi:10.1038/43375

Xu, Q., Zhang, S., & Li, W. (2011). Spatial distribution of large-scale landslides induced by the 5.12 Wenchuan Earthquake. *Journal of Mountain Science, 8*(2), 246-260. doi:10.1007/s11629-011-2105-8

Yuan, Z., Chen, J. e., Owen, L. A., Hedrick, K. A., Caffee, M. W., Li, W., . . . Robinson, A. C. (2013). Nature and timing of large landslides within an active orogen, eastern Pamir, China. *Geomorphology, 182*, 49-65. doi:10.1016/j.geomorph.2012.10.028

Zerathe, S., Lebourg, T., Braucher, R., & Bourlès, D. (2014). Mid-Holocene cluster of large-scale landslides revealed in the Southwestern Alps by ^{36}Cl dating. Insight on an Alpine-scale landslide activity. *Quaternary Science Reviews, 90*, 106-127. doi:10.1016/j.quascirev.2014.02.015